"Adiabatic-hindered-rotor" treatment of the parahydrogen-water complex

Tao Zeng,[1] Hui Li,[2] Robert J. Le Roy,[1] and Pierre-Nicholas Roy[1,a)]
[1]*Department of Chemistry, University of Waterloo, Waterloo, Ontario N2L 3G1, Canada*
[2]*Institute of Theoretical Chemistry, State Key Laboratory of Theoretical and Computational Chemistry, Jilin University, 2519 Jiefang Road, Changchun 130023, People's Republic of China*

(Received 2 June 2011; accepted 2 August 2011; published online 1 September 2011)

Inspired by a recent successful adiabatic-hindered-rotor treatment for parahydrogen pH_2 in CO_2–H_2 complexes [H. Li, P.-N. Roy, and R. J. Le Roy, J. Chem. Phys. **133**, 104305 (2010); H. Li, R. J. Le Roy, P.-N. Roy, and A. R. W. McKellar, Phys. Rev. Lett. **105**, 133401 (2010)], we apply the same approximation to the more challenging H_2O–H_2 system. This approximation reduces the dimension of the H_2O–H_2 potential from 5D to 3D and greatly enhances the computational efficiency. The global minimum of the original 5D potential is missing from the adiabatic 3D potential for reasons based on solution of the hindered-rotor Schrödinger equation of the pH_2. Energies and wave functions of the discrete rovibrational levels of H_2O–pH_2 complexes obtained from the adiabatic 3D potential are in good agreement with the results from calculations with the full 5D potential. This comparison validates our approximation, although it is a relatively cruder treatment for pH_2–H_2O than it is for pH_2–CO_2. This adiabatic approximation makes large-scale simulations of H_2O–pH_2 systems possible via a pairwise additive interaction model in which pH_2 is treated as a point-like particle. The poor performance of the diabatically spherical treatment of pH_2 rotation excludes the possibility of approximating pH_2 as a simple sphere in its interaction with H_2O. © *2011 American Institute of Physics*. [doi:10.1063/1.3626840]

I. INTRODUCTION

The H_2O and H_2 molecules are two of the simplest chemical species. Their mutual interaction is of crucial importance in diverse areas of investigation and is the subject of vigorous research efforts. One field of particular practical interest is the storage of H_2 in H_2O cages (clathrates) (Refs. 1–9), and having a proper understanding of the interaction between H_2 and different cage H_2O structures is of central importance in this area. The H_2–H_2O interaction also plays a significant role in astrophysics, since collisions between these two molecules occur frequently in the interstellar medium, and are responsible for the formation of H_2O masers.[10] Also, the condensation of H_2 onto icy interstellar dust grains is driven by the H_2–H_2O interaction.[11,12] The theoretical study of such macroscopic systems relies largely on molecular simulations, and they require an accurate and efficiently calculated interaction potential between H_2O and H_2.

There have been several attempts to generate accurate potential energy surfaces (PES) for the H_2O–H_2 system via the use of *ab initio* computations.[13–18] Since this system is a typical van der Waals complex, the intramolecular vibrational motions of the covalent H−H and O−H bonds and of the H−O−H angle occur on different time scales than the intermolecular hindered rotations and radial stretching motions of the two moieties. It is therefore wise to freeze or average over those intramolecular vibrational motions to generate a 5-dimensional (5D) rigid rotor PES for the H_2O–H_2 complex if the potential is not used to study processes involving intramolecular vibrational excitation. Four of the five dimensions are the Euler angles that determine the relevant orientation of the two moieties, and the left-over one determines their separation.

The highest level of *ab initio* calculation employed in the works cited above is the CCSD(T)-R12 method employed by Valiron *et al.*[17] In their work, they first generated a reference 5D rigid-rotor PES using the conventional CCSD(T) method[19] with the H_2O and H_2 held at their equilibrium structures. In the next step, they performed explicitly correlated CCSD(T)-R12 (Refs. 20 and 21) calculations to calibrate the original CCSD(T) PES. Furthermore, they performed CCSD(T) calculations for H_2O and H_2 structures with non-equilibrium geometries to generate a 9D PES, and used the ground state vibrational eigenfunctions of the two molecules to average this PES to obtain a 5D PES. The success of such an explicitly correlated and vibrationally averaged PES is demonstrated by the two recent works of Wang and Carrington[22] and van der Avoird and Nesbitt[23] who employed this PES to perform exact bound state calculations for the H_2O–H_2 complex. They both obtained results that were in excellent agreement with experimental data.[24] Despite the success in such a small system, the 5D dimension of this two-body PES is still too high if one is interested in the simulation of many-body systems. The objective of the present work is, therefore, to further reduce the dimension of this PES and to assess the accuracy of such a reduced-dimensional treatment.

H_2 is of special interest because of its bosonic nature, low mass, and weak intermolecular interactions. These three factors make H_2 a good candidate for the observation of superfluidity at low temperatures. *Para*-H_2, whose ground state has zero rotational energy, is more likely to exhibit superfluidity than is *ortho*-H_2, and there have been several theoretical

a)Electronic mail: pnroy@uwaterloo.ca.

studies predicting this special property for pH_2.[25–27] The ground state of a free rotating pH_2 molecule has a non-degenerate $l = 0$ spherical harmonic wave function, and its first excited state is the five-fold degenerate $l = 2$ state with an energy more than 350 cm^{-1} higher than that of the ground state. In this paper, l is reserved for the rotational quantum number of H_2, while j is associated with that of H_2O. This fairly large energy gap suggests that it may be satisfactory to treat the pH_2 molecule in van der Waals complexes diabatically as a sphere.[26,28–31] Under this approximation, performing a simple spherical average over the two degrees of freedom (spherical angles) describing the rotation of H_2 about its centre of mass effectively removes these coordinates, and large-scale simulations become much less expensive. However, such an approximation may be too crude when the interaction between pH_2 and its partner(s) is strong enough to substantially hinder its rotation by mixing the ground rotational state with excited states.[32]

A more accurate yet equally efficient method is to approximate pH_2 as an adiabatic moiety in the potential of its surroundings, i.e., to adiabatically separate the H_2-rotation from the other motions. Application of the adiabatic separation of different degrees of freedom in molecular motions dates back to the "Born-Oppenheimer angular/radial separation" introduced by Holmgren *et al.*[33] to handle atom-diatomic van der Waals complexes more than three decades ago. The same concept was embedded in the "adiabatic bender" approximation of Alexander *et al.*[34–36] about 20 years later. Klopper *et al.* studied HF dimers based on the adiabatic separation of the fast H−F bond stretching from the slow motion of the other degrees of freedom.[37,38] In the first decade of the present century, Leforestier and co-workers performed theoretical studies on the vibration-rotation-tunneling spectroscopy of the H_2O dimer, work that was based on the adiabatic separation of the fast intramolecular vibration and the slow intermolecular rovibrational motion.[39,40] More recently, Li *et al.*[32] first applied the adiabatic separation to the rotation of pH_2 in the CO_2–H_2 van der Waals complex, treating pH_2 as an adiabatic-hindered-rotor (AHR) to generate an effective potential that depends only on the two polar coordinates that determine the relative position between a point-like H_2 and CO_2. Comparisons with the spectroscopic properties generated from their earlier *ab initio* calculation[41] on the CO_2–H_2 complex with the full 4D PES showed that the results from the AHR treatment are an order of magnitude closer to the exact values than those from the diabatically spherical (SPH) treatment, and that the agreement between their AHR and exact results is highly satisfactory. Later, this adiabatic effective potential was successfully applied to study the size evolution of the superfluid response of the pH_2 clusters doped with CO_2.[27]

The success of the AHR CO_2–pH_2 potential inspired us to examine the utility of a similar treatment for the more challenging H_2O–pH_2 system. Ideally, this approximation would remove the two angles that describe the relative orientation of the rigid H_2, and the Valiron 5D PES would be reduced to a new 3D adiabatic effective PES. Considering the fact that the H_2O–H_2 interaction is slightly stronger (235 *vs.* 220 cm^{-1} at the respective global minima) and more anisotropic (the leading interaction is dipole-quadrupole *vs.* quadrupole-quadrupole) than is the CO_2–H_2 interaction, the AHR approximation is potentially even more important for H_2O–H_2, and one may expect a larger AHR-SPH deviation. However, the fact that the rotational constants of H_2O (the largest one is $\sim$30 cm^{-1}) are of the same order of magnitude as that of H_2 ($\sim$60 cm^{-1}), while the rotational constant of CO_2 ($\sim$0.4 cm^{-1}) is much smaller, means that the H_2O rotational level spacings are more similar to those of H_2 than was true for CO_2, and that the time scale for H_2O rotation is similar to that for H_2. Hence, the adiabatic separation between the internal motions of H_2 and H_2O may not be as good as was the case for H_2 and CO_2, and the non-adiabatic coupling between the two moieties may be more significant. In order to test the validity of our AHR treatment, results obtained from the AHR PES are compared with the exact higher dimension rovibrational levels calculated by Wang and Carrington[22] and van der Avoird and Nesbitt.[23]

The present paper is arranged as follows. Section II provides an introduction to our AHR treatment, and other computational details are given in Sec. III. Section IV examines the features of our 3D AHR PES, and compares it to the original 5D PES and to the 3D diabatic SPH PES. Section V presents and discusses our calculated rovibrational levels and wave functions and compares them with the reference calculations. Concluding remarks are given in Sec. VI.

II. ADIABATIC-HINDERED-ROTOR TREATMENT OF PARAHYDROGEN

Before providing details regarding the Hamiltonian operator, we first need to define relevant coordinate systems. The high-level PES presented by Valiron *et al.*[17] pertains to a system consisting of one H_2O and one H_2; the coordinates of their PES are illustrated in Fig. 1(a). In this frame, the spherical coordinates (R, θ, χ) define the position of the centre of mass of H_2 relative to the centre of mass of H_2O, which is taken to be the origin. The angles (θ', ϕ') describe the orientation of H_2 about its centre of mass, with respect to a reference frame parallel to that of H_2O. Note that when $\chi = 0^\circ$ the vector $\vec{R}$ lies in the plane of H_2O, and when $\phi' = 0^\circ$ H_2 lies in the plane parallel to the plane of H_2O.

Our objective is to generate an AHR effective PES that depends only on the position of the centre of mass of pH_2 and treats the pH_2 as a point-like particle. The coordinates of this AHR PES are shown in Fig. 1(b). Wang and Carrington[22] and van der Avoird and Nesbitt[23] employed the coordinates in Fig. 1(c) to calculate the bound-state rovibrational levels of complexes formed by one H_2O with one H_2. Three coordinate frames, the space-fixed frame (SFF), the dimer-fixed frame (DFF), and the water-fixed frame (WFF), were used. Both the SFF and DFF have their origins at the centre of mass of the H_2O–H_2 complex, while WFF takes the centre of mass of H_2O as the origin. The Z'-axis of the DFF points from its origin to the pH_2, while the X'-axis is defined to be perpendicular to the Z'-axis and to lie in the plane containing the Z'-axis and the C_2 symmetry axis of H_2O before rotating the WFF in the DFF. The z'-axis of the WFF lies on the H_2O C_2 axis, and its x'-axis lies in the plane containing the

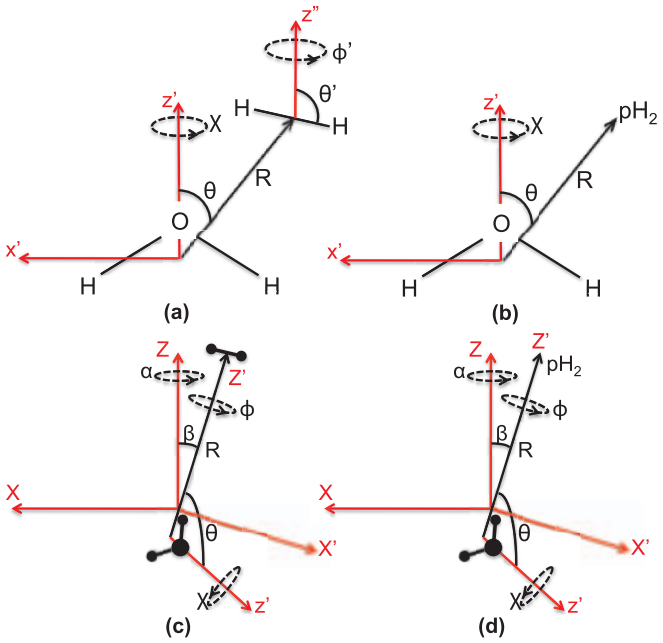

FIG. 1. Coordinates used (a) by Valiron *et al.* (Ref. 17) to generate their PES; (b) in the present work to calculate the AHR effective PES for H_2O–pH_2; (c) by Wang and Carrington (Ref. 22) to calculate the rovibrational levels of the H_2O–H_2 complex; (d) in the present work to calculate the rovibrational levels of the H_2O–pH_2 complex. H_2O and H_2 are represented by black ball-stick model in panels (c) and (d). The axes and coordinates of the H_2-frame are not shown in panel (c), as their relation to the H_2O-frame axes are identical to that shown in panel (a).

three atoms of H_2O. As we go from Fig. 1(a) to 1(b) following the AHR treatment of pH_2, we employ the coordinates in Fig. 1(d) to calculate the rovibrational levels of the H_2O–pH_2 complex. Note the similarity between the coordinates in Fig. 1(d) and those used in the studies of H_2O-(rare gas) atom complexes,[42,43] since they share the same number of effective degrees of freedom.

In Figs. 1(c) and 1(d), α and β are the two Euler angles to rotate the SFF to the DFF, and ϕ, θ, and χ are the three Euler angles to rotate the WFF in the DFF. The first rotation is about the common origin of the SFF and DFF, while the second is about the WFF origin. As noted by van der Avoird and Nesbitt,[23] the values of θ and χ in the frames of Figs 1(a) and 1(b) correspond to the values of θ and $\pi - \chi$ in the frames of Figs. 1(c) and 1(d) because the angles in Figs. 1(c) and 1(d) describe the rotation of the WFF away from the vector $\vec{R}$, while those in panels (a) and (b) describe the rotation of $\vec{R}$ away from the WFF. Nevertheless, due to the C_{2v} symmetry of H_2O, the same θ and χ values found in panels (a) and (b) can be used in panels (c) and (d) to calculate the potential.

The total wave function of the complex is a function of the coordinates described in Fig. 1(c),

$$\Psi(\phi, \theta, \chi, \theta', \phi', R, \alpha, \beta), \tag{1}$$

and the total Hamiltonian operator for the complex is

$$\hat{H}_{\text{total}} = \hat{T}_{H_2O} + \hat{T}_{H_2} - \frac{\hbar^2}{2\mu}\frac{\partial^2}{\partial R^2} + \frac{\hbar^2}{2\mu R^2}\left[\hat{\vec{J}} - \left(\hat{\vec{j}}_{H_2O} + \hat{\vec{j}}_{H_2}\right)\right]^2 + V(R, \theta, \chi, \theta', \phi')$$

$$= \hat{T}_{H_2O} + \hat{T}_{H_2} - \frac{\hbar^2}{2\mu}\frac{\partial^2}{\partial R^2} + \frac{\hbar^2}{2\mu R^2}\left[\hat{J}^2 + \hat{j}^2_{H_2O} + \hat{j}^2_{H_2} + 2\hat{\vec{j}}_{H_2O}\cdot\hat{\vec{j}}_{H_2} - 2\hat{\vec{J}}\cdot\hat{\vec{j}}_{H_2O} - 2\hat{\vec{J}}\cdot\hat{\vec{j}}_{H_2}\right] + V(R, \theta, \chi, \theta', \phi'). \tag{2}$$

All the kinematic operators are written with respect to the DFF. In this expression, $\hat{T}_i$ stands for the rigid rotor kinetic operators for $i = H_2O$ or H_2; $-((\hbar^2/2\mu)(\partial^2/\partial R^2))$ is the kinetic energy for the intermolecular stretching motion and μ is the reduced mass of the H_2–H_2O pair; $\hat{\vec{J}}$ stands for the total angular momentum operator, and $\hat{\vec{j}}_i$ stands for the angular momentum operators of H_2O or H_2. The term in square brackets is the rotational kinetic operator for the DFF.

Our adiabatic approximation originates with the classical Hamiltonian of the system that has the form,

$$H_{\text{total}} = T_{H_2O}(\phi, \theta, \chi, \dot{\phi}, \dot{\theta}, \dot{\chi}) + T_{H_2}(\theta', \phi', \dot{\theta}', \dot{\phi}') + T_{\text{DFF}}(\alpha, \beta, \dot{\alpha}, \dot{\beta}) + \frac{1}{2}\mu\dot{R}^2 + V(R, \theta, \chi, \theta', \phi'), \tag{3}$$

in which T_{DFF} stands for the kinetic energy of the rotation of the DFF in the SFF. The dependence of the rotational kinetic energies on their Euler angles and angular velocities comes from the fact that the angular velocities about the principal rotational axes of a rigid body can be expressed as a linear transformation of the Euler angle velocities, and the transformation is determined by the values of the Euler angles (Eq. (4.125) of Ref. 44 or Eqs. (3.39) and (3.43) of Ref. 45). The moment of inertia of H_2 ($(1/2)m_H r^2_{H_2}$, with an inertial rotational constant of $\sim$60 cm^{-1}) is small compared to both those of H_2O, whose largest rotational constant is around 30 cm^{-1}, and that of the DFF, which is large mainly because of the large value of R compared to r_{H_2} and implies a rotational constant of around 0.7 cm^{-1}.[23] We may, therefore, assume that the angular velocities of the H_2O and DFF rotations are negligibly small compared to those of the H_2. This is equivalent to setting $\dot{\phi} = \dot{\theta} = \dot{\chi} = \dot{\alpha} = \dot{\beta} = 0$, and the T_{H_2O} and T_{DFF} terms in the classical Hamiltonian are correspondingly neglected.

A possible argument against this approximation is that the difference between the H_2 and H_2O moments of inertia is not too large (only a factor of two), so the adiabatic approximation may be ill-posed. However, the adiabatic separation becomes more sound from the viewpoint of quantum mechanics. Because of the restriction on the l quantum numbers (even only) of the rotational states of pH_2, the smallest transition between its rotational levels ($l = 0 \rightarrow l = 2$) occurs around 350 cm^{-1}, which is an order of magnitude larger than the energy of the smallest transition between H_2O rotational levels ($0_{00} \rightarrow 1_{01}$, at about 25 cm^{-1}). This suggests there are different time scales for the rotations of the two species because the typical time scale of a motion is proportional to the reciprocal of the typical transition energy after the motion has been quantized, which is a manifestation of the energy-time uncertainty principle. Thus, the adiabatic approximation may still be valid, up to a point.

Since we are interested in the bound states of the H_2O–H_2 complex whose radial motion cannot be very fast, given the fairly weak van der Waals interaction, it is safe to assume that $\dot{R}$ is negligibly small and to drop the $(1/2)\mu\dot{R}^2$ term. After all the aforementioned approximations are made, only $T_{H_2} + V$ remain in the classical Hamiltonian, and the H_2O merely serves as the source of a potential energy function to adiabatically hinder the H_2 rotation; i.e., the motion of the H_2 rotation is parametrically dependent on the values of R, θ, and χ through the potential. Correspondingly, the total wave function can be written as a product of the H_2 wave function that parametrically depends on its position in the WFF and the wave function of the remaining coordinates, i.e.,

$$\Psi(\phi, \theta, \chi, \theta', \phi', R, \alpha, \beta) = \psi(\theta', \phi'; R, \theta, \chi)\Phi(R, \phi, \theta, \chi, \alpha, \beta), \quad (4)$$

while the adiabatic H_2 state is determined by solving the Schrödinger equation for

$$(\hat{T}_{H_2} + V(R, \theta, \chi, \theta', \phi'))\psi(\theta', \phi'; R, \theta, \chi) = V^{\mathrm{AHR}}(R, \theta, \chi)\psi(\theta', \phi'; R, \theta, \chi). \quad (5)$$

The adiabatic state for the motions of the other degrees of freedom $|\Phi\rangle$ and the total adiabatic energy are obtained by solving the adiabatic Schrödinger equation,

$$\hat{H}_{\mathrm{total}}|\psi\rangle|\Phi\rangle = E|\psi\rangle|\Phi\rangle \quad (6)$$

or the equivalent equation,

$$\langle\psi|\hat{H}_{\mathrm{total}}|\psi\rangle|\Phi\rangle = E|\Phi\rangle. \quad (7)$$

Within the operator $\langle\psi|\hat{H}_{\mathrm{total}}|\psi\rangle$, there is a term

$$\langle\psi|\frac{\hbar^2}{2\mu R^2}\hat{j}^2_{H_2}|\psi\rangle, \quad (8)$$

which is a pure H_2 contribution to the DFF rotation and is also parametrically depends on R. This term can be absorbed into the adiabatic Schrödinger equation for H_2, and the corresponding kinematic effect is thus absorbed into the adiabatic-hindered-rotor potential V^{AHR}. Taking this effect into account, the H_2 adiabatic state is determined by

$$\left(\hat{T}_{H_2} + \frac{\hbar^2}{2\mu R^2}\hat{j}^2_{H_2} + V(R, \theta, \chi, \theta', \phi')\right)\psi(\theta', \phi'; R, \theta, \chi) = V^{\mathrm{AHR}}(R, \theta, \chi)\psi(\theta', \phi'; R, \theta, \chi), \quad (9)$$

and the redefined AHR potential V^{AHR} serves as the potential for the motion of H_2O in the presence of the AHR H_2. One should note that the presence of $(\hbar^2/2\mu R^2)\hat{j}^2_{H_2}$ on the left-hand side of Eq. (9) is solely due to the fact that the angular momentum operator of the DFF is written as a composite operator in the square bracket of Eq. (2). This means that if we wrote the DFF angular momentum operator explicitly in terms of the derivatives with respect to α and β, the $(\hbar^2/2\mu R^2)\hat{j}^2_{H_2}$ term would not appear. Although all calculations described below were performed using the adiabatic potential as obtained from Eq. (9), for future use, we also prepare the adiabatic potential without considering the $(\hbar^2/2\mu R^2)\hat{j}^2_{H_2}$ term.

Further approximations can be made to the adiabatic Hamiltonian operator for H_2O and the DFF: $\langle\psi|\hat{H}_{\mathrm{total}}|\psi\rangle$. After expansion, we have

$$\begin{aligned}\langle\psi|\,\hat{H}_{\mathrm{total}}\,|\psi\rangle = &-\frac{\hbar^2}{2\mu}\langle\psi|\,\frac{\partial^2}{\partial R^2}\,|\psi\rangle + \langle\psi|\,\hat{T}_{H_2O}\,|\psi\rangle \\ &+\frac{\hbar^2}{2\mu R^2}\Big[\hat{J}^2 + \langle\psi|\,\hat{j}^2_{H_2O}\,|\psi\rangle \\ &+2\,\langle\psi|\,\hat{\vec{j}}_{H_2O}\cdot\hat{\vec{j}}_{H_2}\,|\psi\rangle \\ &-2\hat{\vec{J}}\cdot\langle\psi|\,\hat{\vec{j}}_{H_2O}\,|\psi\rangle - 2\hat{\vec{J}}\cdot\langle\psi|\,\hat{\vec{j}}_{H_2}\,|\psi\rangle\Big] \\ &+V^{\mathrm{AHR}}(R, \theta, \chi), \end{aligned} \quad (10)$$

Note that for all operators with the form $\langle\psi|\,\hat{O}\,|\psi\rangle$, the bra $\langle\psi|$ should act after all the derivatives in $\hat{O}$ have been applied to the operand; e.g.,

$$\langle\psi|\,\frac{\partial}{\partial x}\,|\psi\rangle\,f(x) = \left(\langle\psi|\,\frac{\partial}{\partial x}\,|\psi\rangle\right)f(x) + \frac{\partial}{\partial x}f(x), \quad (11)$$

where the parentheses around the inner product ($\langle\rangle$) denotes that the derivative only applies to the parameters of the ket state, and x stands for any arbitrary parameters of $|\psi\rangle$: R, θ, or χ. Because of the purely imaginary nature of the operator $\hat{\vec{j}}_{H_2}$ and the real nature of $|\psi\rangle$, hermiticity guarantees $\langle\psi|\hat{\vec{j}}_{H_2}|\psi\rangle = 0$, so the $-2\hat{\vec{J}}\cdot\langle\psi|\hat{\vec{j}}_{H_2}|\psi\rangle$ term in Eq. (10) vanishes. For pH_2, one can safely expect that the ground eigenstate of Eq. (9) mainly has $l = 0$ character (shown below), and therefore that the $2\langle\psi|\hat{\vec{j}}_{H_2O}\cdot\hat{\vec{j}}_{H_2}|\psi\rangle$ term in Eq. (10) can be neglected. Because of the normalization $\langle\psi|\psi\rangle = 1$, all the terms with the factor $(\langle\psi|\partial/\partial x|\psi\rangle)$ are zero. Since $\hat{\vec{j}}_{H_2O}$ only contains first-derivative operators, $(\langle\psi|\hat{\vec{j}}_{H_2O}|\psi\rangle) = 0$ and $-2\hat{\vec{J}}\cdot\langle\psi|\hat{\vec{j}}_{H_2O}|\psi\rangle = -2\hat{\vec{J}}\cdot\hat{\vec{j}}_{H_2O}$.

If we make the following further approximations:

$$-\frac{\hbar^2}{2\mu}\langle\psi|\,\frac{\partial^2}{\partial R^2}\,|\psi\rangle \approx -\frac{\hbar^2}{2\mu}\frac{\partial^2}{\partial R^2}; \quad (12)$$

$$\langle\psi|\,\hat{T}_{H_2O}\,|\psi\rangle \approx \hat{T}_{H_2O}; \quad (13)$$

$$\langle\psi|\,\hat{j}^2_{H_2O}\,|\psi\rangle \approx \hat{j}^2_{H_2O}, \quad (14)$$

then the adiabatic Hamiltonian operator is reduced to the same form as that for H_2O interacting with a rare gas atom,[42,43]

$$\hat{H}^{\mathrm{BO}} = -\frac{\hbar^2}{2\mu}\frac{\partial^2}{\partial R^2} + \hat{T}_{H_2O} + \frac{\left(\hat{\vec{J}} - \hat{\vec{j}}_{H_2O}\right)^2}{2\mu R^2} + V^{\mathrm{AHR}}(R, \theta, \chi), \quad (15)$$

where the superscript "BO" denotes the resemblance to the Born-Oppenheimer treatment of the nuclear vibration problem on an adiabatic electronic PES. Similarly, in the present work, we ignore all the diagonal adiabatic correction to the kinematic operators and employ $\hat{H}^{\mathrm{BO}}$ to calculate the rovibrational levels of the H_2O–pH_2 complex. The approximation of Eq. (14) is hidden in Eq. (13), as $\hat{T}_{H_2O}$ contains $\hat{j}^2_{H_2O}$, and

the validity of Eqs. (12) and (13) largely depends on the variation of $|\psi\rangle$ with respect to R, θ, and χ, or in another view, on whether the ground state energy of $|\psi\rangle$ lies close to any excited state energy.[46] We find that the ground AHR state $|\psi\rangle$ is well energy-separated from the lowest excited state (by at least 192 cm^{-1}, which is very large compared to the rovibrational transitions presented in Sec. V) at any R, θ, and χ configuration. Thus, one should not expect $|\psi\rangle$ to vary rapidly with respect to its parameters, and the calculated results below confirm the small effect of the diagonal adiabatic correction terms. Note that those diagonal adiabatic correction terms can be added to the calculation as done in Ref. 47, and such a treatment may be performed in the future.

III. COMPUTATIONAL DETAILS

Spherical harmonics $Y_{lm}(\theta', \phi')$ are used as basis functions to solve the AHR equation for H_2 (Eq. (9)). To compare our results with those of van der Avoird and Nesbitt,[23] we use their H_2 rotational constant ($B = 59.3398$ cm^{-1}) in calculating the matrix elements of $\hat{T}_{H_2}$, as well as the same number ($l_{max} = 8$) of spherical harmonic basis functions. Since we are interested in pH_2, only spherical harmonics with even l numbers are used, and we hardly observe any contribution from the basis functions with $l = 6$ or 8 in the ground AHR state $|\psi\rangle$. Gaussian-Legendre and Gaussian-Chebyshev quadratures are used to perform integration over θ' and ϕ', respectively, in the evaluation of potential matrix element,

$$\int \sin\theta' d\theta' \int d\phi' Y_{lm}(\theta', \phi') V(R, \theta, \chi, \theta', \phi') Y_{l'm'}(\theta', \phi'), \tag{16}$$

and 32 and 64 quadrature points are used for θ' and ϕ'. We solve Eq. (9) on a grid of 48 R values ranging from 2.5 to 30 a_0 with a dense distribution around the strong interaction region (5.5–9 a_0), 19 θ values ranging from 0° to 180° with a 10° interval, and 10 χ values ranging from 0° to 90° with a 10° interval. The V^{AHR} values in the mesh holes are obtained by cubic spline interpolation using the V^{AHR} values on the grid, and the V^{AHR} values for $\chi \in (90°, 360°)$ are obtained by considering the C_{2v} symmetry of H_2O and mapping the χ value to the symmetrically identical one in the range [0°, 90°]. Comparison of interpolated V^{AHR} values with the actual ones obtained by solving Eq. (9) showed errors of less than 10^{-4} cm^{-1}. In contrast with the above, if we only use Y_{00} (θ', ϕ') to expand the $|\psi\rangle$, then the eigenvalue of Eq. (9) equals

$$\langle Y_{00}| \hat{T}_{H_2} + \frac{\hbar^2}{2\mu R^2} \hat{j}^2_{H_2} + V(R, \theta, \chi, \theta', \phi') |Y_{00}\rangle, \tag{17}$$

which collapse to the diabatic spherical rotor potential V^{SPH}. The comparison between V^{AHR} and V^{SPH} reveals the anisotropy of the H_2 rotation at the presence of H_2O and the possibility of treating H_2 as a simple sphere in the molecular dynamic studies of the larger H_2O–H_2 systems.

A product of eigenkets of symmetric-top rotations $|jkK\rangle|JKM\rangle$ is used as the elementary angular basis to solve the adiabatic rovibrational Schrödinger equation for the complex,

$$\hat{H}^{BO} |\Phi\rangle = E |\Phi\rangle. \tag{18}$$

$|jkK\rangle$ describes the motion of the WFF in the DFF and $|JKM\rangle$ describes the motion of the DFF in the SFF. M stands for the projection of the total angular momentum J along the SFF Z-axis, and K for the projection along the DFF Z'-axis, while k stands for the projection of the H_2O angular momentum j on the WFF z'-axis (the C_2 axis). After the AHR treatment, pH_2 becomes a point-like particle and H_2O is the only source of rotation about the Z'-axis, and thus the bases $|jkK\rangle$ and $|JKM\rangle$ share the same K value. The common K value in the product basis is closely related to the special character of the Euler angle ϕ in Figs. 1(c) and 1(d). ϕ can be viewed as the third Euler angle of the DFF rotation in SFF or the first Euler angle of the WFF rotation in DFF, and the same angular velocity naturally gives the same projection of the angular momentum on the Z'-axis. Given this picture, one may take this angle as the first Euler angle of the WFF rotation and take the third Euler angle of the DFF rotation to be zero,[22,23,42] or vice versa.[43] We adopt the first point of view, and write the basis set in the space representations as

$$\langle \alpha, \beta, 0|JKM\rangle = \sqrt{\frac{2J+1}{4\pi}} D^J_{MK}(\alpha, \beta, 0)^*; \tag{19}$$

$$\langle \phi, \theta, \chi|jkK\rangle = \sqrt{\frac{2j+1}{8\pi^2}} D^j_{Kk}(\phi, \theta, \chi)^*, \tag{20}$$

where $\{D^J_{MK}\}$ are the Wigner functions.[45]

Since our adiabatic potential $V^{AHR}(R, \theta, \chi)$ does not depend on the orientation in the SFF, $\hat{H}^{BO}$ is isotropic in the SFF, and J and M are good quantum numbers. Also, applying the inversion, operation to V^{AHR} (R, θ, χ) with respect to the centre of mass of the complex will change it to V^{AHR} $(R, \theta, -\chi)$,[22] which is equal to V^{AHR} (R, θ, χ) for the C_{2v} symmetry of the potential in the WFF. Therefore, $\hat{H}^{BO}$ is invariant to the inversion and the associated eigenstates have definite parity. Consequently, our elementary angular basis $|jkK\rangle|JKM\rangle$ can be combined to give a parity-adapted basis,[43]

$$|\Theta^{JMP}_{jkK}\rangle = \frac{1}{\sqrt{2(1+\delta_{K,0}\delta_{k,0})}} \Big[|jkK\rangle |JKM\rangle + (-1)^{J+k+P} |j\ -k\ -K\rangle |J\ -KM\rangle \Big], \tag{21}$$

where if $P = 0$ (1), the basis is even (odd) under the inversion, the quantum numbers that are conserved by $\hat{H}^{BO}$ are superscripts, and δ is the Kronecker δ. The evenness or oddness of k determines whether *para*- or *ortho*-H_2O is considered.[22,23] As in the works of Refs. 22–24, we use the spectroscopic parity e and f to label our adiabatic rovibrational states, and e and f correspond to $(-1)^{J+P} = 1$ and -1. We also use the same number of angular basis functions ($j_{max} = 10$) as did Ref. 23 in order to allow a sensible comparison. For the parity-adapted basis set $\{|\Theta^{JMP}_{jkK}\rangle\}$, the restrictions on the basis indices

are

$$K \geq 0;$$
$$k \geq 0 \quad \text{if } K = 0;$$
$$k \neq 0 \quad K \neq 0 \quad \text{if } (-1)^{J+P} = -1, \tag{22}$$

in order to remove the linear dependent and null bases. For the intermolecular radial stretching, the sine discrete variable representation (DVR) basis[48] $\{R_n\}$ is employed, and there are a total of 45 DVR basis vectors in the range [4 a_0, 26 a_0], which is identical to the selection of Wang and Carrington.[22] The eigenstates of $\hat{H}^{\mathrm{BO}}$ are expanded in the space of the radial-angular product basis $\{|R_n\rangle|\Theta^{JMP}_{jkK}\rangle\}$.

The matrix elements of the second and third operators in Eq. (15) can be obtained by adapting the general formulas of Brocks *et al.*[49] to our parity-adapted basis, and they are given in the Appendix without detailed derivation. The radial kinetic operator matrix element in the DVR basis is standard (Eq. (A6) of Ref. 48), and is not given here. The same H_2O rotational constants are used as in Ref. 23: $A = 27.8806\ \mathrm{cm}^{-1}$, $B = 14.5216\ \mathrm{cm}^{-1}$, and $C = 9.2778\ \mathrm{cm}^{-1}$, to calculate the matrix element of $\hat{T}_{\mathrm{H_2O}}$. They are the ground vibrational state rotational constants for the rotations about the x'-, z'-, and y'-axis in the WFF, and are taken from Ref. 50. The masses of the H and O atoms are chosen to be 1.007825 and 15.994915u, respectively, as in Ref. 23. For the matrix element of V^{AHR}, 13 Gaussian-Legendre and 26 Gaussian-Chebyshev quadrature points are used for the numerical integration over θ and χ. The treatment of the matrix element of V^{AHR} is also briefly described in the Appendix.

The eigenvalues and eigenvectors are obtained through the Lanczos algorithm.[51–53] We performed convergence tests and found that the rovibrational energies converge to $10^{-4}\ \mathrm{cm}^{-1}$ with the present choice of quadrature points and sizes of angular and radial basis sets. Although the Coriolis interaction in the third operator of Eq. (15) couple bases with different K (Eq. (A1)) and V^{AHR} couples bases with different j (Eqs. (A6)–(A8)), we still try assigning K and $j_{K_aK_c}$ labels to the eigenstates of $\hat{H}^{\mathrm{BO}}$ as Wang and Carrington did.[22] The comparison with their assignments can be used to judge the quality of our adiabatic wave functions. The approach used for K assignments is the same as in Ref. 22, and is not detailed here. All states of concern in this work have principal K values of 0 or 1, and they are labeled as Σ and Π states, respectively. For the $j_{K_aK_c}$ assignment, since Wang and Carrington found that most of the pH$_2$ states have H_2O rotation with quantum number $j = 0$ or 1, we do not perform the general unitary transformation for the eigenstate into the $|j_{K_aK_c}\rangle$ basis as they did. Rather, we simply apply the projection operators $|0_{00}\rangle\langle 0_{00}|$, $|1_{10}\rangle\langle 1_{10}|$, $|1_{11}\rangle\langle 1_{11}|$, and $|1_{01}\rangle\langle 1_{01}|$ to the eigenstate to pick out the corresponding components.

Another way to assess our wave functions is to calculate the transition line strengths between the rovibrational levels and compare with results in Ref. 22. The transition line strength between two states is defined as

$$S_{i'i} = 3 \sum_{M',M} |\langle \Phi'_i | \mu_Z^{\mathrm{SFF}} | \Phi_i \rangle|^2. \tag{23}$$

One should note that there is a typographical error in the definition of line strength in Eq. (9) of Ref. 22, where the summation $\sum_{M',M}$ is mispositioned in the operation of taking the absolute square. Here, μ_Z^{SFF} is the electric dipole operator along the SFF Z-axis. For the case of a H_2O-(rare gas) complex, the formula for the matrix element $\langle J'K'M'|\langle j'k'K'|\mu_0^{\mathrm{SFF}}|jkK\rangle|JKM\rangle$ has been worked out by Hutson (Eq. (30) of Ref. 42), and we adapt his formula to our parity-adapted basis. The matrix element formula is also given in the Appendix.

IV. THE AHR EFFECTIVE POTENTIAL

Before examining our AHR potential, we should recall some features of the Valiron PES. It has one global minimum and one local minimum.[17] The global minimum lies at $R = 5.82\ a_0$, $\theta = 0°$, and $\theta' = 0°$, with a binding energy of 234.15 cm^{-1}; the local minimum lies at $R = 6.07\ a_0$, $\theta = 119°$, $\chi = 0°$, $\theta' = 90°$, and $\phi' = 90°$, with a binding energy of 199.40 cm^{-1}. Note that the θ' and ϕ' angles in this section are defined with respect to a H_2-frame that rotates along with $\vec{R}$ and has its z''-axis pointing along $\vec{R}$ in the WFF. This is illustrated in the coordinates of Fig. 2(b), and one should not take the values of θ' and ϕ' in Fig. 1(a) as defining the local minimum. Given the new frame, one can see that the local minimum has H_2 perpendicular to the plane of H_2O. Using the terminology of Zhang *et al.*,[15] the global minimum is called the H_2 proton donor (H_2PD) configuration and the local minimum H_2 proton acceptor (H_2PA) configuration.

In stark contrast to the 5D PES, V^{AHR} does not have any minimum corresponding to the H_2PD configuration, and its only minimum is quite close to the H_2PA configuration, with $\theta = 110°$ and $\chi = 0°$. Since the θ' and ϕ' degrees of freedom are lost after the AHR (or SPH) treatment, the term "configuration" only refers to a set of R, θ, and χ values, and this is different from the discussion of the 5D PES above. Contour plots of the V^{AHR} and V^{SPH} minima are shown in Fig. 3, with their corresponding R values being plotted in Fig. 4. At $\theta = 0°$ (corresponding to the H_2PD configuration before the adiabatic treatment), the V^{AHR} value is more than 20 cm^{-1} higher than the global minimum, which is at $\theta = 110°$, $\chi = 0°$, and $R = 6.35\ a_0$. This orientation is close to the 5D H_2PA configuration.

This change of global minimum from the 5D PES to V^{AHR} can be explained by examining the potential surfaces in Fig. 2. Figure 2(a) clearly indicates that any H_2 rotation away from the $\theta' = 0°$ H_2PD configuration increases the potential energy steeply. This strongly localized minimum must correspond to a very large kinetic energy, because of the uncertainty principle. In contrast, Fig. 2(b) demonstrates a low energy trough for the rotation about the z''-axis when $\theta' = 90°$. This low-energy trough attenuates the kinetic pressure[54,55] and lowers the V^{AHR} value. This can also be explained in light of the wavefunction. The ground state of a pH$_2$ hindered rotor must have a mainly $l = 0$ character that equally samples all orientations of θ' and ϕ', and the one low-energy H_2PD configuration makes little contribution to V^{AHR}. On the other hand, the low-energy trough in Fig. 2(b)

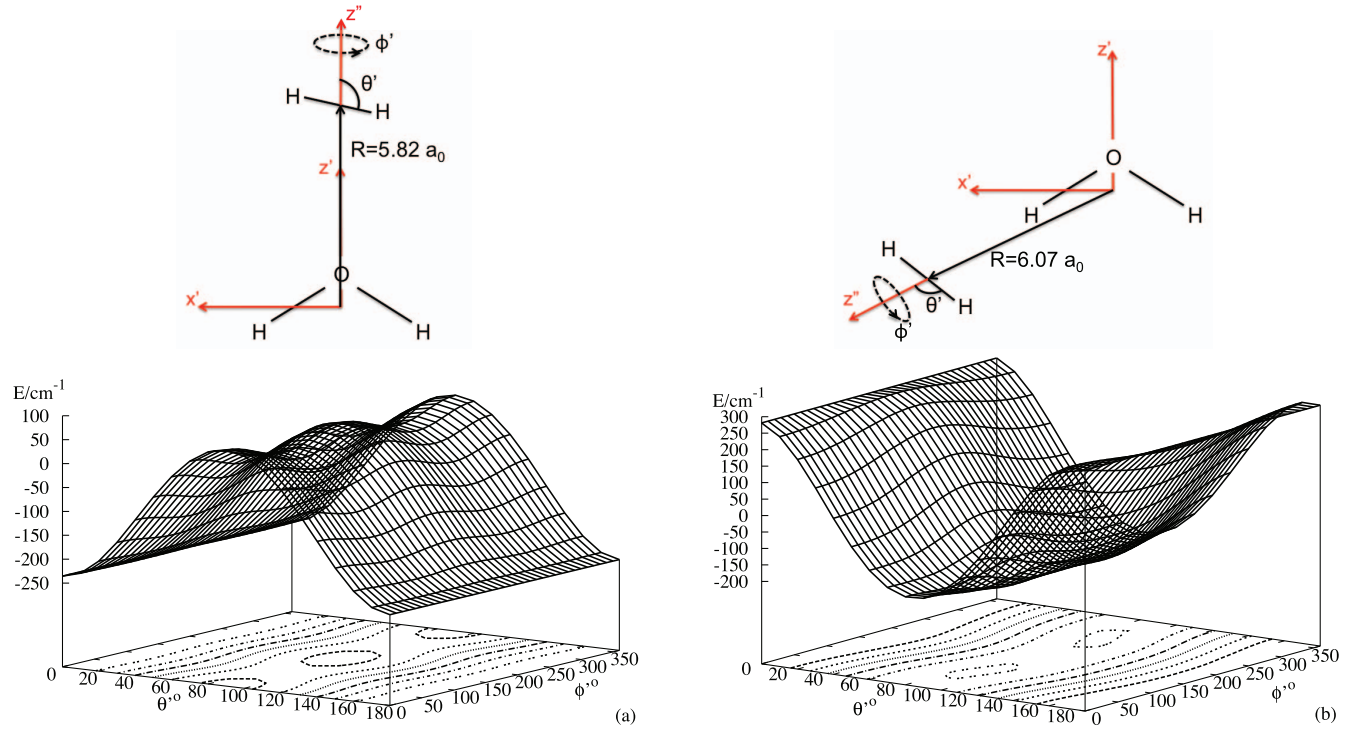

FIG. 2. Potential energy surfaces as functions of the solid angles (θ',ϕ') of H_2: (a) at the global minimum and (b) at the local minimum of the Valiron PES. Note the difference between the z'' axis orientations in panel (b) and Fig. 1(a) (see text).

provides many more low energy configurations of θ' and ϕ' to be sampled by the spherical wave function and leads to the lower V^{AHR}. According to Zhang *et al.*,[15] the H_2PA configuration is stabilized by the bond-pair electrons of H_2 interacting with the electropositive hydrogen atom of H_2O. Apparently this interaction does not change substantially along with rotation of the H_2 bond about the O−H bond axis, and the low-energy trough is formed.

The pH_2 AHR ground state wave function at the H_2PD configuration can be decomposed to be

$$0.9357s + 0.0639d + 0.0003g, \tag{24}$$

while the one at the H_2PA configuration is

$$0.9239s + 0.0757d + 0.0004g, \tag{25}$$

in which the conventional atomic spectrum symbols s, d, and g are used to label spherical harmonics with $l = 0$, 2, and 4. The coefficients are the probabilities of the respective components, and should not be misunderstood as the basis set coefficients in wave function expansions. These compositions confirm the mainly s-character in the pH_2 AHR rotor and the negligible contributions from functions with $l > 4$, as mentioned before. The distribution densities of the two states are illustrated in Fig. 5. The low-value surfaces reveal the dominant s-character in both cases, while the high-value ones reflect the mixing in of d-character. Because of the C_{2v} symmetry of the H_2O-potential at the H_2PD configuration, only the d_0 basis is of the same irreducible representation as the s basis and can mix in the ground state to form the d_z^2-type distribution in Fig. 5(a). This distribution reflects the polarization of the H_2 distribution (from a sphere to a quadrupole) in the presence of the H_2O to have greater sampling of the $\theta' = 0°$ low-energy configuration. In the present work, the word "polarization" is used to describe the change of pH_2 rotational wave function in the presence of its interaction partner and should not be misunderstood as electric or magnetic polarization in the usual sense.

Another s-d polarization is observed at the H_2PA configuration, as is illustrated in Fig. 5(b). The d-contribution, which looks like a "lifesaver" around the z''-axis, mainly comes from the d_2- and d_{-2}- (or d_{xy}- and $d_{x^2-y^2}$-) components that peak in the plane perpendicular to the z''-axis (the x''-y'' plane). Obviously, this d-type distribution corresponds to H_2 rotation in the low-energy trough of the H_2PA PES, and increases the sampling of such low-energy configurations. The larger equilibrium intermolecular distance (R_e) at the H_2PA configuration after the AHR treatment (6.35 *vs.* 6.07 a_0) reflects the weaker anisotropy for the larger R,[17] which leads to the flatter PES of Fig. 2(b) with both a higher minimum (low-energy trough) and a lower maximum (high-energy edge) that favours the equal sampling of (θ', ϕ') configurations by the s-component of the AHR wave function.

The difference between V^{SPH} and V^{AHR} is more significant than in similar comparison for the CO_2-pH_2 complex.[32] For that species, the two types of PES have similar topographies, and their minima differ only by 8.15 cm^{-1}. However, Fig. 3 shows significantly different topographies between V^{SPH} and V^{AHR}, as V^{SPH} has its minimum at $\theta = 76°$, $\chi = 0°$, and $R = 6.17$ a_0, while that of V^{AHR} lies at $\theta = 110°$, $\chi = 0°$, and $R = 6.35$ a_0. Furthermore, the difference between the energies of the AHR and SPH minima (−97.56 vs. −78.70 cm^{-1}) is more than twice as large as that for the CO_2 complex. This large difference is attributed to the fact that since it has a permanent dipole, the H_2O molecule is expected

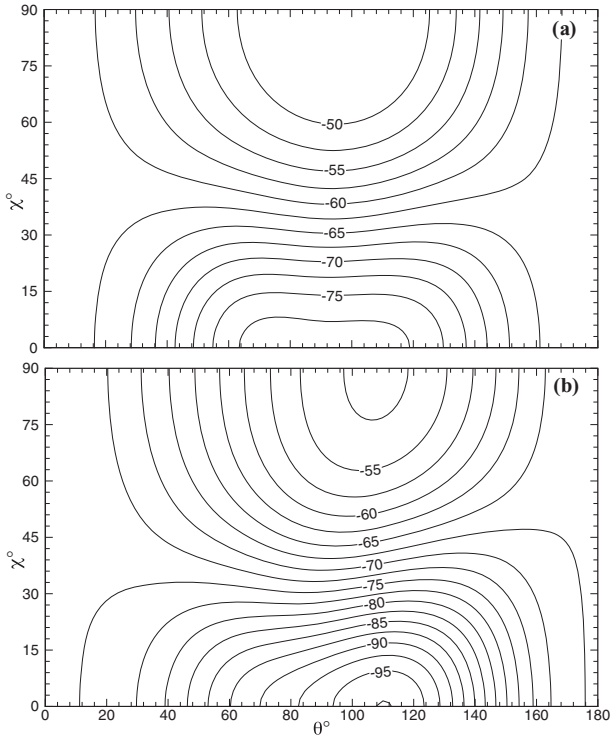

FIG. 3. Contour plots of the minimum energy of (a) V^{SPH} and (b) V^{AHR} in the symmetrically unique orientation in the WFF. The range of χ is restricted to $[0^\circ, 90^\circ]$ because of the C_{2v} symmetry of H_2O. All energies are minimized with respect to R.

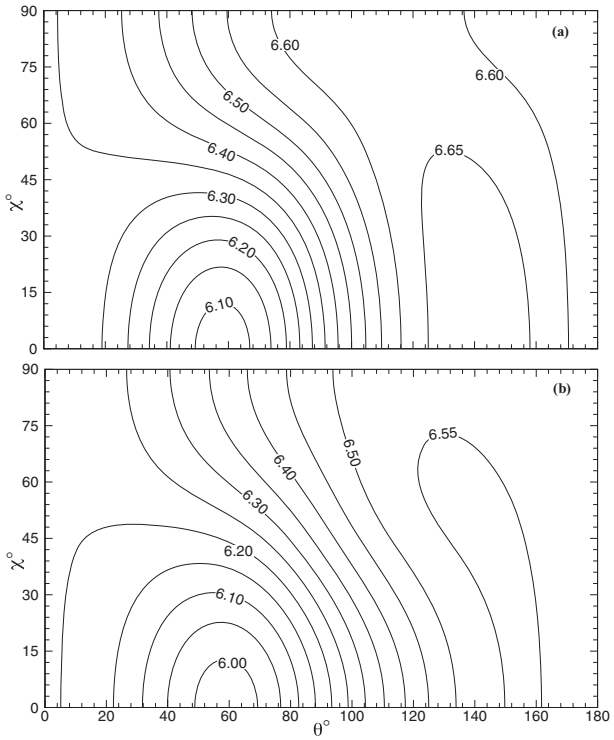

FIG. 4. Contour plots of the R values that minimize (a) V^{SPH} and (b) V^{AHR} in Fig. 3.

to polarize the distribution of the $p\mathrm{H}_2$ more than does the CO_2 molecule, which has only a quadrupole moment, and thus more polarization energy is obtained. This is also consistent with the larger d-contributions seen in Eqs. (24) and (25), compared to the negligible contribution in the CO_2 complex, for which it is always smaller than 2%. Figure 4 shows that for a given orientation (θ, χ), the equilibrium intermolecular distance of the AHR complex is about 0.1 a_0 shorter than the SPH, a result consistent with the stronger interaction. Overall, the substantial difference between the AHR and SPH potential energies excludes the possibility of treating $p\mathrm{H}_2$ as a diabatic sphere[26,28–31] in its interaction with H_2O.

V. ROVIBRATIONAL LEVELS OF THE AHR POTENTIAL

This section presents our calculation of the rovibrational levels of the H_2O–$p\mathrm{H}_2$ complexes using V^{AHR}, and compares them with the exact calculations. Note that the word "exact" in the following discussion is associated with the results of computations based on the full 5D Valiron PES.[22,23] It should not be mistaken for highly accurate experimental data or theoretical results obtained without any approximation. We focus on comparisons of the calculated energy levels and wave functions. The quality of our adiabatic wave functions Ψ is judged based on their reproducibility of the K- and $j_{K_a K_c}$-assignments, of the 2D probability densities, and of the transition line strengths yielded by the exact wave functions.

A. Adiabatic rovibrational energy levels

The calculated bound-state rovibrational levels for $p\mathrm{H}_2\mathrm{O}$–$p\mathrm{H}_2$ and *ortho*-H_2O–$p\mathrm{H}_2$ are summarized in Tables I and II. These tables have the same format as Tables II and III of Ref. 23, and the 5D reference values are also listed to facilitate comparison. The correlations between our calculated levels and the reference levels are also plotted in Figs. 6 and 7 to provide a visual comparison. The energy zero for the two tables is the potential (V^{AHR}, V^{SPH}, or the Valiron 5D potential for the respective tabulated energies) energy value at the dissociation limit as $R \to \infty$. First of all,

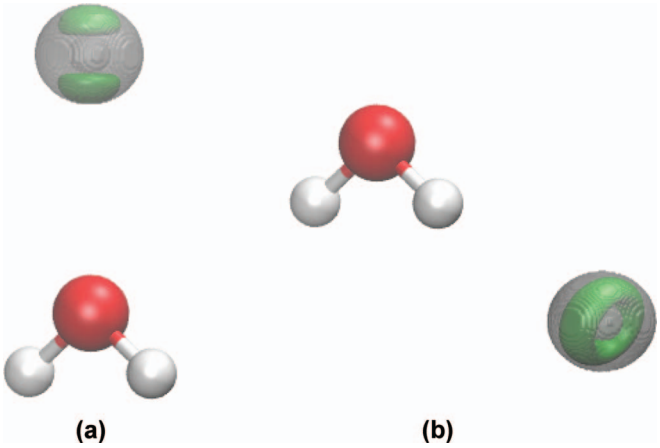

FIG. 5. Distribution density isosurfaces of the AHR ground state of $p\mathrm{H}_2$ at the (a) H_2PD and (b) H_2PA configurations. The gray surface has the value of 0.005, and the interior green one 0.08, representing the low- and high-value surfaces.

TABLE I. Bound state rovibrational levels of *para*-H_2O–pH_2 in cm^{-1}. All states have more than 99% Σ-character. Spectroscopic parity and $j_{K_aK_c}$ labels are also used to characterize the states. The intermolecular stretching vibrationally excited state is denoted by asterisk. The level energies calculated using V^{SPH} are in parenthesis. For comparison, the reference exact results from van der Avoird and Nesbitt (Ref. 23) are given in italic font under the AHR results.

Σ ($K = 0$) Parity ($j_{K_aK_c}$)	$J = 0$		$J = 1$		$J = 2$		$J = 3$		$J = 4$		$J = 5$	
e (0_{00})	–34.7485	(–28.1011)	–33.3526	(–26.7837)	–30.5745	(–24.1638)	–26.4424	(–20.2732)	–21.0020	(–15.1636)	–14.3219	(–8.9152)
	–33.5663		*–32.1841*		*–29.4334*		*–25.3431*		*–19.9596*		*–13.3528*	
e (0_{00})∗	–2.2974	(–0.9854)	–1.6167	(–0.4509)	–0.3305	(0.5143)						
	–2.0615		*–1.3979*		*–0.1628*							

we see that the AHR energy levels are qualitatively consistent with the exact results, as we can unambiguously associate the AHR levels with the exact levels, and there are no bound f states for the *para*-H_2O–pH_2 complex in our calculation. All of the adiabatic levels are lower than the corresponding exact levels, as illustrated in Figs. 6 and 7 where all the AHR correlation points lie below the $y = x$ line. This is not inconsistent with the variational principle, since an approximation has been introduced to the Hamiltonian operator (from Eq. (10) to Eq. (15)), and not only to the wave function.

The largest deviations occur for the ground states of the two systems (*para*- and *ortho*-H_2O complexes), which are $-1.1822\ cm^{-1}$ for the $J = 0\ \Sigma^e$ state of the *para*-H_2O complex and $-1.4349\ cm^{-1}$ for the $J = 0\ \Sigma^e$ state of the *ortho*-H_2O complex. These values amount to 3.5% and 11.2% errors when they are divided by the ground state energies from van der Avoird and Nesbitt.[23] All reported percent errors in this work are with respect to the exact results, i.e., deviation divided by the reference value. While the former error is fairly small, the large 11.2% error seems to indicate that the AHR treatment is too crude for the *ortho*-H_2O–H_2 complex. However, when the $-1.4349\ cm^{-1}$ error is divided by the binding energy $\mathcal{D}_0$ of the exact calculation for such a state (i.e., by $36.6336\ cm^{-1}$), the percent error decreases to 3.9%. Note that the dissociation limit of the *ortho*-H_2O–pH_2 complex corresponds to an *ortho*-H_2O with a ground state rotational energy of $23.7994\ cm^{-1}$, and this should be added to the energy levels to calculate $\mathcal{D}_0$,[23] whereas the *para*-H_2O–pH_2 complex has no rotational energy at the dissociation limit, and its $\mathcal{D}_0$ is equal to the negative of its ground state energy. The similar $\mathcal{D}_0$ percent errors tend to indicate the AHR model works for both systems. The fact that the ground states have the largest error is consistent with the observation for the CO_2–pH_2 AHR vibrational spectrum (see Table II of Ref. 32). This is because the ground states have the shortest intermolecular distance and the strongest coupling between the motions of the two molecules, which makes the adiabatic approximation crudest for such cases. The largest CO_2–pH_2 ground-state error

TABLE II. Bound state rovibrational levels of *ortho*-H_2O–pH_2 in cm^{-1}. The dissociation limit has an energy of $23.8994\ cm^{-1}$. The percentages of the Σ- and Π-characters are shown in parentheses following the level energies, if they are smaller than 99%. Spectroscopic parity and $j_{K_aK_c}$ labels are also used to characterize the states. The intermolecular stretching vibrationally excited state is denoted by asterisk. For comparison, the reference exact results from van der Avoird and Nesbitt (Ref. 23) are given in italic font under the AHR results.

Σ ($K = 0$) Parity ($j_{K_aK_c}$)	$J = 0$	$J = 1$	$J = 2$	$J = 3$	$J = 4$	$J = 5$
e (1_{01})	–14.2781	–13.4541 (92%)	–11.5886 (82%)	–8.5158 (76%)	–4.1740 (70%)	1.4344 (66%)
	–12.8342	*–12.0544 (91%)*	*–10.2452 (81%)*	*–7.2284 (74%)*	*–2.9472 (69%)*	*2.5914 (65%)*
e (1_{01})∗	21.6806	21.6620 (63%)	22.3268 (56%)	23.5609 (52%)		
	21.9456	*21.8911 (60%)*	*22.5298 (55%)*	*23.7161 (51%)*		
f (1_{10})	14.7927	16.4902 (97%)	19.8011 (91%)			
	15.6570	*17.3383 (97%)*	*20.6180 (91%)*			
Π ($K = 1$) Parity ($j_{K_aK_c}$)	$J = 0$	$J = 1$	$J = 2$	$J = 3$	$J = 4$	$J = 5$
e (1_{01})		–6.3640 (92%)	–2.6740 (83%)	2.5120 (76%)	9.0342 (71%)	16.7436 (67%)
		–5.4371 (91%)	*–1.7436 (81%)*	*3.4203 (74%)*	*9.8971 (69%)*	*17.5393 (66%)*
e (1_{10})		6.2275	9.0370	13.2215	18.7417	
		7.3546	*10.1354*	*14.2761*	*19.7355*	
e (1_{01})∗		23.4756 (64%)				
		23.6188 (62%)				
f (1_{01})		–6.9588	–4.2775	–0.1690	5.1660	11.7009
		–6.0622	*–3.3522*	*0.6738*	*5.9645*	*12.4420*
f (1_{10})		5.8621 (97%)	8.0058 (91%)	11.3125 (86%)	15.8219 (81%)	21.5368 (76%)
		6.9922 (97%)	*9.1140 (91%)*	*12.3878 (86%)*	*16.8523 (81%)*	*22.5087 (76%)*
f (1_{01})*		22.8335				
		22.9665				

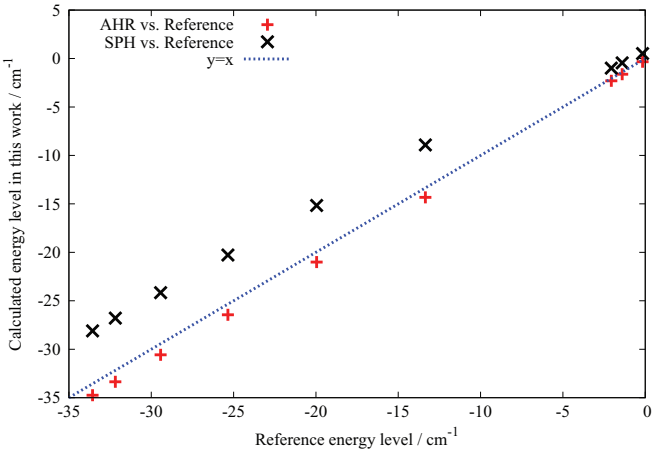

FIG. 6. Correlations between the AHR rovibrational bound state levels for the pH$_2$O–pH$_2$ complex and reference results (Ref. 23). The SPH values are also included for comparison purposes.

is 0.404 cm^{-1}, which is only 0.7% of the ground state binding energy.[32] Thus, it is clear that the AHR model is distinctly cruder for the H$_2$O–pH$_2$ complexes.

Since chemistry is more concerned with energy differences, rather than absolute energy values, we use the two ground-state levels as zero points to calculate the excitation energies for all the bound states in Tables I and II, and compare with the results obtained through similar calculations using the data of van der Avoird and Nesbitt.[23] Since all the adiabatic levels are systematically lower than the exact levels, these errors are partially cancelled in calculating such excitation energies. The largest errors of this type are 1.0145 cm^{-1} for the $J = 3$ Σ^e* state of the *para*-H$_2$O complex, and 1.3019 cm^{-1} for the $J = 1$ Π^f* state of the *ortho*-H$_2$O complex, corresponding to 3.0% and 3.6% errors, respectively, similar to the corresponding $\mathcal{D}_0$ percent errors. Most of the percent errors for other levels are smaller than these two values, with the exceptions of the lowest Π^e and Π^f states of the *ortho*-H$_2$O complex with $J = 1$–3. The percent errors for those states decrease as J increases, and the maximum errors are 7.9% for the lowest $J = 1$ Π^f state and 6.9% for the lowest $J = 1$ Π^e state. The similarity of these errors for the Π^e and Π^f states are understandable, as their parity splitting is small (discussed below). The large percent errors are caused by the relatively small excitation energies (7.4061 and 6.7810 cm^{-1} from Ref. 23) for the two transitions, despite the relatively small absolute errors (0.5080 and 0.5383 cm^{-1}). Therefore, they do not invalidate our approximation, and the agreement between our adiabatic excitation energies and the exact results is generally good.

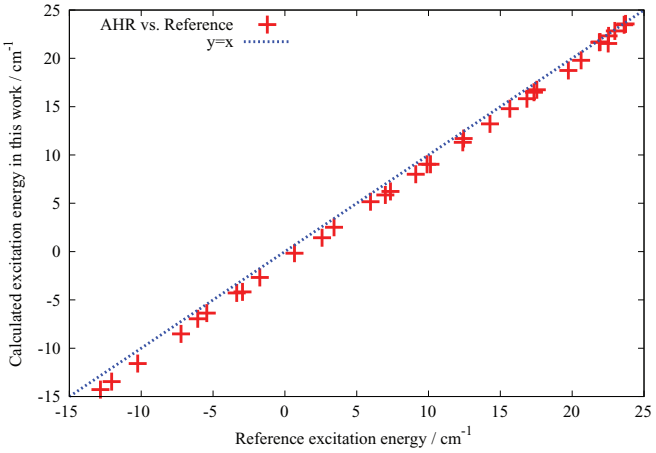

FIG. 7. Correlations between the AHR rovibrational bound state levels for the oH$_2$O–pH$_2$ complex and reference results (Ref. 23).

For comparison, we also calculated the rovibrational levels for the *para*-H$_2$O complex using V^{SPH}, and the results are included in Table I (numbers in parentheses). In accordance with its shallower potential well depth (see Fig. 3), the energies of the states with the ground intermolecular vibrational state are much higher than the AHR (exact) levels by about 6 (5) cm^{-1}. The AHR-SPH deviations for the intermolecular vibrational excited states are much smaller, by about 1 cm^{-1}. This is because the two moieties are farther apart for the radial excited states, and the H$_2$ rotation is less hindered. However, the $J = 2$ Σ^e* state becomes unbound when V^{SPH} is used. Thus, the unsuitability of the SPH treatment for pH$_2$ rotation in spectroscopic calculations is clearly demonstrated. Similar SPH calculations were also carried out for the *ortho*-H$_2$O complex, and the deviations there are even larger. Moreover, some SPH levels cannot even be unambiguously associated with the exact levels. In view of this poor performance, the SPH treatment is not discussed further here.

B. Adiabatic rovibrational wave functions

The first criterion for the quality of our adiabatic wave functions is the accuracy of jK_aK_c level assignments. These assignments fully agree with those of Wang and Carrington,[22] and this confirms that our wave functions capture the H$_2$O rotational character correctly. Wang and Carrington did not give the percentage of the main $j_{K_aK_c}$ components in each wave function, and neither do we. However, all the assigned $j_{K_aK_c}$ components contribute more than 94% to the adiabatic wave functions, and the assignments are unambiguous. The almost pure H$_2$O rotational component in each wave function tends to suggest that the H$_2$O rotation is also adiabatically hindered in the presence of pH$_2$, and consequently, that an AHR treatment could also be applied to H$_2$O. However, because of the much smaller energy spacings between the H$_2$O rotational levels, coupling between different rotational levels is very likely to happen in the presence of more than one pH$_2$, so we see little point in developing potentials with both H$_2$O and pH$_2$ treated using the AHR approach.

The K-assignments also parallel those of van der Avoird and Nesbitt.[23] We reproduce not only the principal K-value for each state, but also its percent contribution to the wave function, with the largest error being 3% (our 63% *vs.* their 60% for the $J = 1$ Σ^e* state of the *ortho*-H$_2$O complex). An interesting observation in Table II is the pairwise K-component percentages for the Σ and Π states in the same intermolecular vibrational level with the same $j_{K_aK_c}$ symbol and spectroscopic parity. For example, the Σ^e (1_{01}) state has 92%, 82%, and 76% of Σ-contributions for $J = 1$, 2, and

3, and the corresponding Π^e (1_{01}) state has 92%, 83%, and 76% of Π-contributions; the Σ^e* (1_{01}) state makes a 63% Σ-contribution for $J = 1$, and the corresponding Π^e* (1_{01}) state makes a 64% Σ-contribution. This pattern clearly indicates that there is little contribution from basis functions with $K \geq 2$ for the bound states, and that the mixing of K-components only happens between Σ and Π states. The neglect of the higher K-components is due to there being negligible contributions from $j > 1$ H_2O rotational states (K being bounded by j) in the wave functions, as they require excitation energies that are larger than the dissociation energies of the two complexes. On the other hand, the $C^+_{J,K}$ and $C^-_{J,K}$ values increase as J increases, and so does the Coriolis coupling (see Eq. (A1)). Consequently, the Σ-Π mixing increases as J increases, and this leads to a monotonic declining of the percentage of the principal K-component, as is observed in Table II.

Obviously, the parity splitting is all due to terms with $(-1)^P$ in Eqs. (A1), (A3), (A6), and (A7). Since the $(-1)^P$ term in the matrix elements of $\hat{T}_{H_2O}$ and V^{AHR} is always associated with a $\delta_{K,0}$ factor, one can come up with a two-step parity splitting scheme for the Π states as follows. The first step comes from the parity-dependent Coriolis mixings with the Σ states. The second comes from the Σ-components in the already split Π^e and Π^f states, which respond parity-dependently to $\hat{T}_{H_2O}$ and V^{AHR}. This scheme suggests that the larger the Σ-Π mixing, the larger the parity splitting for the Π states, and this is consistent with the fact that from $J = 1$–5, the splitting between the Π^e (1_{01}) and Π^f (1_{01}) states increases from 0.5949 to 5.0427 cm^{-1}, along with an increase of the Σ-contribution from 8% to 33% in the Π^e state. As seen in the preceding subsection, when the parity splitting is small for these two states at $J = 1$, they even have similar errors in excitation energies compared to the exact values.

In accordance with the conclusion of van der Avoird and Nesbitt,[23] only one quantum of intermolecular vibration can be excited within the bound states; we label all of these intermolecular vibrational excited states by an asterisk in Tables I and II. Whether the state is an intermolecular vibrational excited state or not is judged by examining the radial distribution function,

$$P(R) = \int \sin\beta d\beta \int d\alpha \int \sin\theta d\theta \int d\phi \times \int d\chi \, \Phi(R, \phi, \theta, \chi, \alpha, \beta)^* \Phi(R, \phi, \theta, \chi, \alpha, \beta). \quad (26)$$

The resultant distribution functions for the $J = 0$ Σ^e and Σ^e* states of the *para*-H_2O complex are plotted in Fig. 8. Although the bimodal structure of the radial distribution for the Σ^e* state is obvious, one may still argue that it is not a pure vibrational excited state since the radial distribution does not go to zero and a true radial node is absent. In fact, the excited state has 5% contribution of the H_2O 1_{11} rotational state, so it is also partially a rotational excited state. Consequently, the position of the nodal plane must have some dependence on the orientation (θ, χ), and for every orientation the radial node lies at a slightly different R value. This orientational smearing of the radial node yields the apparently nodeless radial distribution for the Σ^e* state shown in Fig. 8. However, this does not impair our assignment for the radial vibrational states, since the radial excitation is always dominant compared to the associated rotational excitation for the asterisk-denoted states. The radial distributions for the other states are similar to the two typical cases in Fig. 8, with slight differences regarding the peak and node positions. Depending on the purity of the rotational components of the radial excited states, their radial distribution may have a true node.

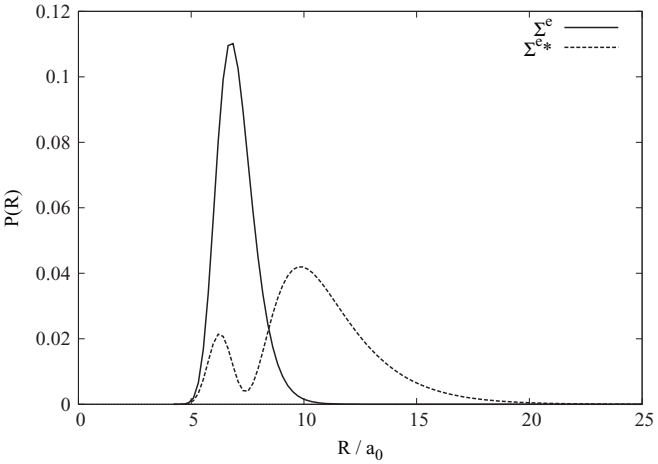

FIG. 8. Radial distribution functions for the $J = 0$ Σ^e and Σ^e* states of the *para*-H_2O–*p*H_2 complex. They were obtained from calculations with 100 radial DVR bases in order to obtain smooth curves.

In order to obtain an overall image of how well our adiabatic wave functions represent the distribution of the *p*H_2 around the H_2O, we compute the 2D orientational distribution function,

$$P(\theta, \chi) = \int \sin\beta d\beta \int d\alpha \int d\phi \int dR \Phi(R, \phi, \theta, \chi, \alpha, \beta)^* \times \Phi(R, \phi, \theta, \chi, \alpha, \beta), \quad (27)$$

for the four ground states of the two parities for each of the two types of H_2O complexes; the resulting contour plots are presented in Fig. 9. The lowest-energy f state of the *para*-H_2O complex, a pure Σ^f state, is not bound, and thus has no entry in Table I. When these four panels are compared with the distributions of the corresponding states from the exact calculations of Wang and Carrington (Figs. 8(a)–8(d)),[22] the

TABLE III. Line strengths (in units $\mu_{H_2O}{}^2$) for transitions between rovibrational levels of the *para*-H_2O–*para*-H_2 complex. The labels and energies (AHR and exact) of the $J = 1$ levels are given in the header row, and those of the $J = 2$ levels in the first column. The reference results of Wang and Carrington (Ref. 22) for both energies and line strengths are given in parentheses. The symbols after the line strengths are associated with the transitions shown in Fig. 10.

	$\Sigma^e(0_{00})$ − 33.3640 (−32.194)	$\Sigma^e(0_{00})*$ −1.6207 (−1.400)
$\Sigma^e(0_{00})$ − 30.5855 (−29.443)	0.0003 (0.0006) b	0.0198 (0.0181) f
$\Sigma^e*(0_{00})$ − 0.3334(−0.163)	0.0531 (0.0366) g	0.0000 (0.0000)

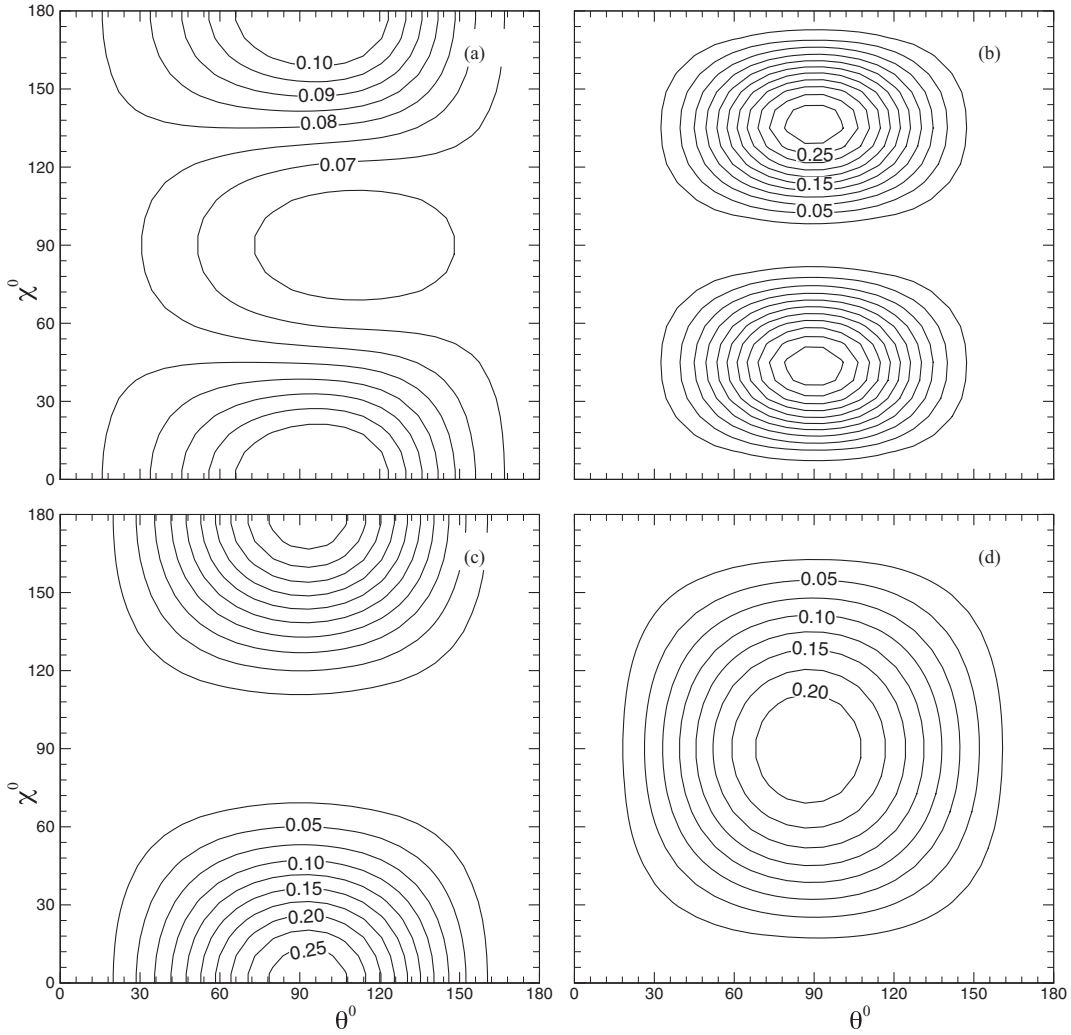

FIG. 9. The angular distribution function $P(\theta, \chi)$ for the lowest energy $J = 0$ states of the (a) e and (b) f parities of the *para*-H_2O complex, and (c) e and (d) f parities of the *ortho*-H_2O complex.

differences between the two sets of contour plots are not discernible. The pH_2 distribution around a H_2O molecule is well represented by our adiabatic wave functions, a result that is very important for future studies of large clusters of H_2 with our AHR treatment.

Finally, we calculated the transition line strengths between some rovibrational levels and compare with the results of Wang and Carrington.[22] The results (in units of $\mu^2_{H_2O}$) are summarized in Tables III and IV. These two tables have the same format as Tables IX and X of Ref. 22, and the reference results are given (in parentheses) to facilitate comparisons. The transition energies and line strengths in the two tables are plotted in Fig. 10 to provide a visual comparison. We employed the H_2 and H_2O rotational constants used in Ref. 22 to prepare $V^{\rm AHR}$ and the adiabatic wave functions $\{\Phi\}$ for the line strength calculations, in order to have a more sensible comparison. Correspondingly, the energies in Tables III and IV are slightly different from those in Tables I and II, but their deviations from the reference results of Wang and Carrington[22] are similar to those reported in the previous subsection. Some of our line strengths are very different from the exact results, as our values can be twice as large (0.00048 *vs.* 0.00021 in Table IV) or twice as small (0.00079 *vs.* 0.00153 in Table IV). However, those exact line strengths are very small

TABLE IV. Line strengths (in units $\mu_{H_2O}{}^2$) for transitions between rovibrational levels of the *ortho*-H_2O–pH_2 complex. The labels and energies (AHR and exact) of the $J = 1$ levels are given in the header row, and those of the $J = 2$ levels in the first column. The reference results of Wang and Carrington (Ref. 22) for both energies and line strengths are given in parentheses. "x" means that this transition is forbidden. The symbols after the line strengths are associated with the transitions shown in Fig. 10.

	$\Pi^f(1_{01}) - 6.9743(-6.077)$	$\Sigma^e(1_{01}) - 13.4716(-12.071)$	$\Pi^e(1_{01}) - 6.3795(-5.452)$
$\Sigma^e(1_{01}) - 11.6057(-10.261)$	×	0.00008 (0.00003) a	0.00079 (0.00153) d
$\Pi^e(1_{01}) - 2.6894(-1.759)$	×	0.00048 (0.00021) e	0.00130 (0.00244) c
$\Pi^f(1_{01}) - 4.2427(-3.367)$	0.00230 (0.00386) b	×	×

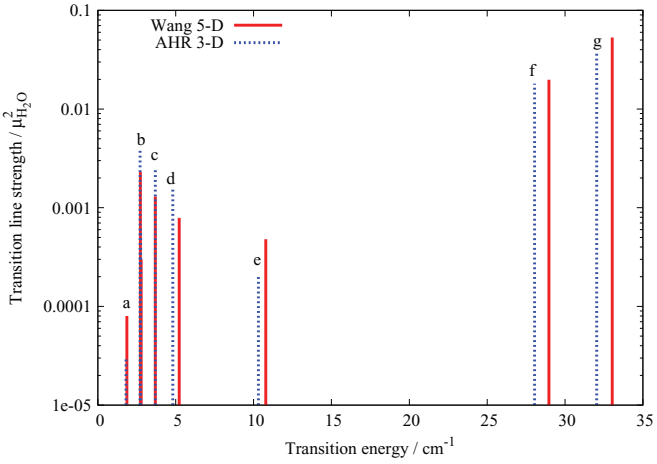

FIG. 10. The transition energies and line strengths in Tables III and IV. The symbols on top of the AHR lines associate with the entries in the two tables.

in magnitude ($\lesssim 10^{-2}$), and, therefore, are very sensitive to wave function error. Moreover, taking the square of the matrix element to obtain the transition line strengths amplifies the deviations. All considered, we are satisfied by the fact that our adiabatic line strengths are qualitatively consistent with the reference values, as they have comparable orders of magnitude.

VI. CONCLUDING REMARKS

We have presented an adiabatic-hindered-rotor treatment for $p\mathrm{H_2}$ in its interaction with $\mathrm{H_2O}$. This approximation is based on the assumption that the $p\mathrm{H_2}$ rotation is much faster than the motions of other degrees of freedom, and can therefore be adiabatically separated out. After making this approximation we solve the Schrödinger equation for the $\mathrm{H_2}$ rigid-rotor taking the other degrees of freedom as parameters, and the resultant eigenvalues form the effective adiabatic potential for the motion of $\mathrm{H_2O}$ in the presence of an adiabatically hindered $p\mathrm{H_2}$ rotor. This approximation reduces the dimension of the original rigid-rotor $\mathrm{H_2O}$–$\mathrm{H_2}$ potential from 5D to 3D and leads to a substantial reduction in computational effort. A thorough examination of the resultant adiabatic potential shows striking differences from the original 5D potential. In particular, the original global minimum associated with the $\mathrm{H_2}$ proton donor configuration disappears, and the new global minimum is associated with the $\mathrm{H_2}$ proton acceptor configuration. This difference can be understood in terms of the optimization of the AHR ground states at the two configurations.

The accuracy of this adiabatic approximation is tested via calculation of the bound-state rovibrational levels of the $\mathrm{H_2O}$–$p\mathrm{H_2}$ complexes, and the results are very convincing. Most of the adiabatic level energies lie within 1 cm^{-1} of the exact energies, and the few exceptions are associated with large excitation energies, and have small percent errors. Computational spectroscopists may think of these errors as being large. However, in the interest of the high computational efficiency brought by the adiabatic approximation, we consider that this sacrifice of accuracy is acceptable. The $j_{K_a K_c}$- and K-assignments of our adiabatic wave functions are quantitatively consistent with the exact results, and the contour plots of the 2D $\mathrm{H_2}$ distribution functions around $\mathrm{H_2O}$ are indiscernible from the exact distributions. The transition line strengths calculated from the adiabatic wave functions are qualitatively consistent with those yielded by the exact wave functions, despite their small values and high sensitivity to wave function error. These observations lead to the conclusion that the wave functions based on our adiabatic-hindered-rotor treatment are very accurate and can be used for calculating system properties and corrections based on perturbation theory that include matrix elements of the adiabatic wave functions. We also compare the diabatically spherical treatment with the adiabatic-hindered-rotor treatment and find much larger differences between those two approximations than was the case for the $\mathrm{CO_2}$–$p\mathrm{H_2}$ complex. We attribute this to the stronger polarization of the $p\mathrm{H_2}$ rotation by the $\mathrm{H_2O}$ dipole compared to the $\mathrm{CO_2}$ quadrupole. The poor performance of the diabatically spherical treatment excludes the possibility of treating $p\mathrm{H_2}$ as a simple sphere in molecular simulations of $\mathrm{H_2O}$–$p\mathrm{H_2}$ systems.

We plan to use our accurate new 3D AHR potential in Feynman path integral simulations of water-doped $p\mathrm{H_2}$ clusters. The removal of the rotational degrees of freedom for the $p\mathrm{H_2}$ molecule allows one to avoid use of the corresponding high-temperature density matrices (Eq. (2.39) of Ref. 56) in path integral simulations, which are highly resource-consuming to evaluate and store as the number of $p\mathrm{H_2}$ molecules grows. Also, application of the efficient pair-product action approximation[57] is straightforward for an ensemble of point-like $p\mathrm{H_2}$. Thus, the validation of the AHR approximation in the present work paves the way for subsequent large-scale path integral studies.

ACKNOWLEDGMENTS

We are grateful to Professor Tucker Carrington, Jr. and Dr. X.-G. Wang for helpful discussions and for sharing an early version of Ref. 22. We thank Professor van der Avoird for providing us with a preprint of Ref. 23, and Dr. Alexandre Faure for providing us with the Valiron PES. Finally, we need to thank Professor Jeremy M. Hutson for enlightening discussions. This research has been supported by the Natural Sciences and Engineering Research Council of Canada (NSERC), by the Canada Foundation for Innovation (CFI), and by the National Natural Science Foundation of China (Grant No. 21003058). We thank the Shared Hierarchical Academic Research Computing Network (SHARCNET) for computing time.

APPENDIX: MATRIX ELEMENTS USED IN THIS PAPER

The matrix element of the DFF rotation operator in our parity-adapted basis reads

$$\left\langle \Theta^{JMP}_{j'k'K'} \right| \langle R_m | \frac{(\hat{\vec{J}} - \hat{\vec{j}})^2}{2\mu R^2} | R_n \rangle \left| \Theta^{JMP}_{jkK} \right\rangle$$

$$= \frac{\hbar^2}{2\mu R_n^2} \frac{\delta_{j',j}\delta_{m,n}}{\sqrt{(1+\delta_{K',0}\delta_{k',0})(1+\delta_{K,0}\delta_{k,0})}}$$

$$\times\{D_{JjK}\delta_{K',K}\left(\delta_{k',k}+(-1)^{J+k+P}\delta_{-k',k}\delta_{K,0}\right)$$
$$-C^{+}_{J,K}C^{+}_{j,K}\delta_{K',K+1}(\delta_{k',k}+(-1)^{J+k+P}\delta_{-k',k}\delta_{K,0})$$
$$-C^{-}_{J,K}C^{-}_{j,K}\delta_{K',K-1}\left(\delta_{k',k}+(-1)^{J+k+P}\delta_{-k',k}\delta_{K,1}\right)\Big\} \quad \text{(A1)}$$

where $D_{JjK}=J(J+1)+j(j+1)-2K^2$ and $C^{\pm}_{J,K}=\sqrt{J(J+1)-K(K\pm1)}$. Note that there is a typographical error in Eq. (42) of Ref. 49, where $+(1/2\mu R^2)$ should be $-(1/2\mu R^2)$, and Eq. (A1) incorporates this correction. The rigid-rotor operator of H_2O is

$$\hat{T}_{H_2O}=\left(\frac{A+C}{2}\right)\hat{j}^2+\left[B-\left(\frac{A+C}{2}\right)\right]\hat{j}^2_{z'}+\left(\frac{A-C}{4}\right)(\hat{j}^2_{+}+\hat{j}^2_{-}), \quad \text{(A2)}$$

where A, B, and C are the rotational constants of H_2O with the conventional definition,[58] and $\hat{j}_{\pm}=\hat{j}_{x'}\mp i\hat{j}_{y'}$ because of the anomalous commutators[45] of the angular momentum operators in the WFF (Fig. 1(d)). The matrix elements of this operator are

$$\left\langle\Theta^{JMP}_{j'k'K'}\middle|\left\langle R_m\middle|\hat{T}_{H_2O}\middle|R_n\right\rangle\middle|\Theta^{JMP}_{jkK}\right\rangle$$
$$=\frac{\delta_{m,n}\delta_{j',j}\delta_{K',K}}{\sqrt{(1+\delta_{K',0}\delta_{k',0})\left(1+\delta_{K,0}\delta_{k,0}\right)}}\Bigg\{\left[\left(\frac{A+C}{2}\right)\times j\,(j+1)+\left(B-\frac{A+C}{2}\right)k^2\right]\times\left(\delta_{k',k}+(-1)^{J+k+P}\delta_{K,0}\delta_{k',-k}\right)$$
$$+\frac{A-C}{4}\left[C^{+}_{j,k}C^{+}_{j,k+1}\left(\delta_{k',k+2}+(-1)^{J+k+P}\delta_{K,0}\delta_{-k',k+2}\right)+C^{-}_{j,k}C^{-}_{j,k-1}\left(\delta_{k',k-2}+(-1)^{J+k+P}\delta_{K0}\delta_{-k',k-2}\right)\right]\Bigg\}. \quad \text{(A3)}$$

We do not calculate the matrix elements of V^{AHR} with the basis directly. Instead, we consider the formula of the multiplication of the V^{AHR} matrix with the coefficient vector of the basis, i.e.,

$$\underline{u}=\underline{\underline{V}}^{AHR}\,\underline{v}\ , \quad \text{(A4)}$$

which is an essential step in the Lanczos algorithm.[51] Here, the single underline denotes a column vector and the double underline denotes a matrix. Since V^{AHR} is independent of ϕ, it conserves the K-value of a pair of basis vectors, and since it depends on the value of R and not on its derivative, it is diagonal in the radial DVR basis. Thus, the multiplication in Eq. (A4) can be performed separately for each group of basis functions with particular values of n and K, i.e.,

$$\underline{u}^{nK}=\underline{\underline{V}}^{AHR,n}\,\underline{v}^{nK}\ . \quad \text{(A5)}$$

For compactness, the formulas for this multiplication are given without derivation in the following:

1. $K=0$ and $J+P$ even,
$$u^{n0}_{j'k'}=\sum_{il}T^{0,\cos}_{il,j'k'}V_n(\theta_l,\chi_i)\sum_{jk}T^{0,\cos}_{il,jk}v^{n0}_{jk}\ ; \quad \text{(A6)}$$

2. $K=0$ and $J+P$ odd,
$$u^{n0}_{j'k'}=\sum_{il}T^{0,\sin}_{il,j'k'}V_n(\theta_l,\chi_i)\sum_{jk}T^{0,\sin}_{il,jk}v^{n0}_{jk}\ ; \quad \text{(A7)}$$

3. $K\neq0$,
$$u^{nK}_{j'k'}=\frac{1}{2}\Bigg[\sum_{il}T^{K,\cos}_{il,j'k'}V_n(\theta_l,\chi_i)\sum_{jk}T^{K,\cos}_{il,jk}v^{nK}_{jk}+\sum_{il}T^{K,\sin}_{il,j'k'}V_n(\theta_l,\chi_i)\sum_{jk}T^{K,\sin}_{il,jk}v^{nK}_{jk}\Bigg], \quad \text{(A8)}$$

in which l and i are the indices for the Gaussian-Legendre (GL) and Gaussian-Chebyshev (GC) quadrature grids, $V_n(\theta_l,\chi_i)$ is the value of $V^{AHR}(R_n,\theta_l,\chi_i)$ and $T^{K,\sin}_{il,jk}$ and $T^{K,\cos}_{il,jk}$ are the transformation matrices connecting the sin and cos representations in our $\{|\Theta^{JMP}_{jkK}\rangle\}$ basis to the angular DVR basis in the angles θ_l and χ_i. θ_l and χ_i are the angles corresponding to the GL and GC grids, i.e., $\theta_l=\arccos(x^{GL}_l)$ and $\chi_i=\arccos(x^{GC}_i)$. The transformation matrices have the definition,

$$T^{K,\sin}_{il,jk}=\sqrt{\frac{w^{GL}_l(2j+1)}{n_\chi(1+\delta_{K,0}\delta_{k,0})}}\sin(k\chi_i)d^{j}_{Kk}\ (\theta_l)\ , \quad \text{(A9)}$$

with a similar one for $T^{K,\cos}_{il,jk}$. In these definitions, $\{w^{GL}\}$ are the weights for the GL quadrature, n_χ is the number of the GC grid points in $[-1,1]$, corresponding to $\chi_i\in[0,\pi]$, and $d^{j}_{Kk}\ (\theta)$ is the Wigner small d function (Eq. (3.57) of Ref. 45). Note that the dependence on $(-1)^P$ in Eqs. (A1), (A3), (A6), and (A7) is the source of the parity splitting in the rovibrational spectrum of the H_2O–pH_2 complexes. The last matrix element we need is for the transition dipole moment along the SFF Z-axis, and it reads

$$\left\langle\Theta^{JMP}_{j'k'K'}\middle|\left\langle R_m\middle|\mu^{SFF}_Z\middle|R_n\right\rangle\middle|\Theta^{JMP}_{jkK}\right\rangle=\frac{\mu_{H_2O}\delta_{m,n}}{2\sqrt{(1+\delta_{k',0}\delta_{K',0})\left(1+\delta_{k,0}\delta_{K,0}\right)}}\delta_{M',M}\ (-1)^{k'+M}[j][j'][J][J']$$
$$\times\begin{pmatrix}J' & 1 & J\\ -M & 0 & M\end{pmatrix}\sum_{\sigma=-1}^{1}\begin{Bmatrix}\begin{pmatrix}j' & 1 & j\\ -k' & 0 & k\end{pmatrix}\begin{pmatrix}j' & 1 & j\\ -K' & \sigma & K\end{pmatrix}\begin{pmatrix}J' & 1 & J\\ -K' & \sigma & K\end{pmatrix}$$

$$+(-1)^{J+P+k}\begin{pmatrix} j' & 1 & j \\ -k' & 0 & -k \end{pmatrix}\begin{pmatrix} j' & 1 & j \\ -K' & \sigma & -K \end{pmatrix}\begin{pmatrix} J' & 1 & J \\ -K' & \sigma & -K \end{pmatrix}$$
$$+(-1)^{J'+P'+k'}\begin{pmatrix} j' & 1 & j \\ k' & 0 & k \end{pmatrix}\begin{pmatrix} j' & 1 & j \\ K' & \sigma & K \end{pmatrix}\begin{pmatrix} J' & 1 & J \\ K' & \sigma & K \end{pmatrix}$$
$$+(-1)^{J+J'+P+P'+k+k'}\begin{pmatrix} j' & 1 & j \\ k' & 0 & -k \end{pmatrix}\begin{pmatrix} j' & 1 & j \\ K' & \sigma & -K \end{pmatrix}\begin{pmatrix} J' & 1 & J \\ K' & \sigma & -K \end{pmatrix}\Bigg\}, \quad \text{(A10)}$$

where $[j] = \sqrt{2j+1}$, the Wigner 3-j symbol is used, and μ_{H_2O} stands for the magnitude of the H_2O electric dipole moment.

[1] W. L. Vos, L. W. Finder, R. J. Hemley, and H. k. Mao, Phys. Rev. Lett. **71**, 3150 (1993).
[2] S. Patchkovskii and J. S. Tse, Proc. Natl. Acad. Sci. U.S.A. **100**, 14645 (2003).
[3] K. A. Kokshin, Y. Zhao, D. He, W. L. Mao, H. k. Mao, R. J. Hemley, M. V. Lobanov, and M. Greenblatt, Phys. Rev. Lett. **93**, 125503 (2004).
[4] L. J. Florusse, C. J. Peters, J. Schoonman, K. C. Hester, C. A. Koh, S. F. Dec, K. N. Marsh, and E. D. Sloan, Science **306**, 469 (2004).
[5] W. L. Mao and H. k. Mao, Proc. Natl. Acad. Sci. U.S.A. **101**, 708 (2004).
[6] W. L. Mao, H. k. Mao, A. F. Goncharov, V. V. Struzhkin, Q. Guo, J. Hu, J. Shu, R. J. Hemley, M. Somayazulu, and Y. Zhao, Science **297**, 2247 (2002).
[7] V. V. Struzhkin, B. Militzer, W. L. Mao, H. k. Mao, and R. J. Hemley, Chem. Rev. **107**, 4133 (2007).
[8] H. Lee, J. W. Lee, D. Y. Kim, J. Park, Y.-T. Seo, H. Zeng, I. L. Moudrakovski, C. I. Ratcliffe, and J. A. Ripmeester, Nature (London) **434**, 743 (2005).
[9] Y. H. Hu and E. Ruckenstein, Angew. Chem., Int. Ed. **45**, 2011 (2006).
[10] T. R. Phillips and S. Green, Astrophys. Space Sci. **224**, 537 (1995).
[11] H. G. Hixson, M. J. Wojcik, M. S. Devlin, J. P. Devlin, and V. Buch, J. Chem. Phys. **97**, 753 (1992).
[12] V. Buch and J. P. Devlin, J. Chem. Phys. **94**, 4091 (1991).
[13] H. Lischka, Chem. Phys. **2**, 191 (1973).
[14] A. Moroz, R. L. Sweany, and S. L. Whittenburg, J. Phys. Chem. **94**, 1352 (1990).
[15] Q. Zhang, L. Chenyang, Y. Ma, F. Fish, M. M. Szczesniak, and V. Buch, J. Chem. Phys. **96**, 6039 (1992).
[16] M. P. Hodges, R. L. Wheatley, G. K. Schenter, and A. H. Harvey, J. Chem. Phys. **120**, 710 (2004).
[17] P. Valiron, M. Wernli, A. Faure, L. Wiesenfeld, C. Rist, S. Kedžuch, and J. Noga, J. Chem. Phys. **129**, 134306 (2008).
[18] P. R. P. Barreto, V. W. Ribas, and F. Palazzetti, J. Phys. Chem. A **113**, 15047 (2009).
[19] K. Raghavachari, G. W. Trucks, J. A. Pople, and M. Head-Gordon, Chem. Phys. Lett. **157**, 479 (1989).
[20] J. Noga, W. Kutzelnigg, and W. Klopper, Chem. Phys. Lett. **199**, 497 (1992).
[21] J. Noga and W. Kutzelnigg, J. Chem. Phys. **101**, 7738 (1994).
[22] X.-G. Wang and T. Carrington, Jr., J. Chem. Phys. **134**, 044313 (2011).
[23] A. van der Avoird and D. J. Nesbitt, J. Chem. Phys. **134**, 044314 (2011).
[24] M. J. Weida and D. J. Nesbitt, J. Chem. Phys. **110**, 156 (1999).
[25] P. Sindzingre, D. M. Ceperley, and M. L. Klein, Phys. Rev. Lett. **67**, 1871 (1991).
[26] Y. Kwon and K. B. Whaley, Phys. Rev. Lett. **89**, 273401 (2002).
[27] H. Li, R. J. Le Roy, P.-N. Roy, and A. R.W. McKellar, Phys. Rev. Lett. **105**, 133401 (2010).
[28] C. Piccarreta and F. A. Gianturco, Eur. Phys. J. D. **37**, 93 (2006).
[29] F. Paesani and K. B. Whaley, J. Chem. Phys. **124**, 234310 (2006).
[30] S. Moroni, M. Botti, S. De Palo, and A. R.W. McKellar, J. Chem. Phys. **122**, 094314 (2005).
[31] H. Zhu and D. Xie, J. Comput. Chem. **30**, 841 (2009).
[32] H. Li, P.-N. Roy, and R. J. Le Roy, J. Chem. Phys. **133**, 104305 (2010).
[33] S. L. Helmgren, M. Waldman, and W. Klemperer, J. Chem. Phys. **67**, 4414 (1977).
[34] M. H. Alexander, S. Gregurick, P. J. Dagdigian, G. W. Lemire, M. J. McQuaid, and R. C. Sausa, J. Chem. Phys. **101**, 4547 (1994).
[35] M. H. Alexander and M. Yang, J. Chem. Phys. **103**, 7956 (1995).
[36] M. H. Alexander, J. Chem. Phys. **108**, 4467 (1998).
[37] W. Klopper, M. Quack, and M. A. Suhm, Chem. Phys. Lett. **261**, 35 (1996).
[38] W. Klopper, M. Quack, and M. A. Suhm, J. Chem. Phys. **108**, 10096 (1998).
[39] C. Leforestier, F. Gatti, R. S. Fellers, and R. J. Saykally, J. Chem. Phys. **117**, 8710 (2002).
[40] C. Leforestier, R. van Harrevelt, and A. van der Avoird, J. Phys. Chem. A **113**, 12285 (2009).
[41] H. Li, P.-N. Roy, and R. J. Le Roy, J. Chem. Phys. **132**, 214309 (2010).
[42] J. M. Hutson, J. Chem. Phys. **92**, 157 (1990).
[43] L. Wang and M. Yang, J. Chem. Phys. **129**, 174305 (2008).
[44] H. Goldstein, *Classical Mechanics*, 2nd ed. (Addison-Wesley, Reading, MA, 1980).
[45] R. N. Zare, *Angular Momentum: Understanding Spatial Aspects in Chemistry and Physics* (Wiley, New York, 1988).
[46] I. B. Bersuker, *The Jahn-Teller Effect* (Cambridge University Press, Cambridge, England, 2006).
[47] F. Gatti and C. Iung, Phys. Rep. **484**, 1 (2009).
[48] D. T. Colbert and W. H. Miller, J. Chem. Phys. **96**, 1982 (1992).
[49] G. Brocks, A. van der Avoird, B. T. Sutcliffe, and J. Tennyson, Mol. Phys. **50**, 1025 (1983).
[50] F. C. DeLucia, P. Helminger, R. L. Cook, and W. Gordy, Phys. Rev. A **5**, 487 (1972).
[51] C. Lanczos, J. Res. Natl. Bur. Stand. **45**, 255–282 (1950).
[52] H. Köppel, L. S. Cederbaum, and W. Domcke, J. Chem. Phys. **77**, 2014 (1982).
[53] A. Nauts and R. E. Wyatt, Phys. Rev. Lett. **51**, 2238 (1983).
[54] K. Ruedenberg and M. W. Schmidt, J. Phys. Chem. A **113**, 1954 (2009).
[55] K. Ruedenberg and M. W. Schmidt, J. Comput. Chem. **28**, 391 (2007).
[56] D. Marx and M. H. Müser, J. Phys.: Condens. Matter **11**, R117 (1999).
[57] D. M. Ceperley, Rev. Mod. Phys. **67**, 279 (1995).
[58] P. R. Bunker and P. Jensen, *Molecular Symmetry and Spectroscopy*, 2nd ed. (National Research Council of Canada, Washington, DC, 1998).